AGU PUBLICATIONS

JGR

Journal of Geophysical Research: Earth Surface

RESEARCH ARTICLE
10.1002/2015JF003634

Key Points:
- Residential (commercial) buildings reduce overwash deposition by 40% (90%)
- Development effectively filters high-frequency overwash events
- Model results predict that reduction in overwash deposition leads to island drowning

Supporting Information:
- Texts S1 and S2, Figures S1a–S1g, and Table S1

Correspondence to:
L. J. Moore,
laura.moore@unc.edu

Citation:
Rogers, L. J., L. J. Moore, E. B. Goldstein, C. J. Hein, J. Lorenzo-Trueba, and A. D. Ashton (2015), Anthropogenic controls on overwash deposition: Evidence and consequences, *J. Geophys. Res. Earth Surf.*, *120*, 2609–2624, doi:10.1002/2015JF003634.

Received 9 JUN 2015
Accepted 12 NOV 2015
Accepted article online 13 NOV 2015
Published online 29 DEC 2015

Anthropogenic controls on overwash deposition: Evidence and consequences

Laura J. Rogers[1], Laura J. Moore[1], Evan B. Goldstein[1], Christopher J. Hein[2], Jorge Lorenzo-Trueba[3], and Andrew D. Ashton[4]

[1]Department of Geological Sciences, University of North Carolina at Chapel Hill, Chapel Hill, North Carolina, USA, [2]Department of Physical Sciences, Virginia Institute of Marine Science, College of William and Mary, Gloucester Point, Virginia, USA, [3]Department of Earth and Environmental Studies, Montclair State University, Montclair, New Jersey, USA, [4]Department of Geology and Geophysics, Woods Hole Oceanographic Institution, Woods Hole, Massachusetts, USA

Abstract Accelerated sea level rise and the potential for an increase in frequency of the most intense hurricanes due to climate change threaten the vitality and habitability of barrier islands by lowering their relative elevation and altering frequency of overwash. High-density development may further increase island vulnerability by restricting delivery of overwash to the subaerial island. We analyzed pre-Hurricane Sandy and post-Hurricane Sandy (2012) lidar surveys of the New Jersey coast to assess human influence on barrier overwash, comparing natural environments to two developed environments (commercial and residential) using shore-perpendicular topographic profiles. The volumes of overwash delivered to residential and commercial environments are reduced by 40% and 90%, respectively, of that delivered to natural environments. We use this analysis and an exploratory barrier island evolution model to assess long-term impacts of anthropogenic structures. Simulations suggest that natural barrier islands may persist under a range of likely future sea level rise scenarios (7–13 mm/yr), whereas developed barrier islands will have a long-term tendency toward drowning.

1. Introduction

Barrier islands are narrow, low-elevation landforms that are highly sensitive to changes in sea level and storm activity. The population densities of barrier islands along the Atlantic and Gulf Coasts of the U.S. are, on average, 3 times greater than those of coastal states and are increasing [*Zhang and Leatherman*, 2011]. Additionally, tourism is the largest business sector in the world and coastal tourism, including on barrier islands, is the greatest segment of that global industry [*Honey and Krantz*, 2007]. Much of the attraction to barrier islands stems from their natural beauty and abundance of recreational opportunities, a consequence of their low elevation, typically only ~2 m above sea level [*Psuty*, 2002].

The same characteristics that make barrier islands popular places to live and visit also make them especially vulnerable to changing environmental conditions. Conservative estimates predict that global sea level will rise between 28 and 61 cm by 2100 [*Stocker et al.*, 2013]. Further, evidence reveals that the U.S. mid-Atlantic coastline, where barrier islands dominate the shore, is a sea level rise (SLR) hot spot, with current SLR rates on the order of 3–4 times the global average [*Sallenger et al.*, 2012]. Incorporating local SLR and Intergovernmental Panel on Climate Change Representative Concentration Pathway 8.5 projections, *Kopp et al.* [2014] suggest a SLR of 0.7–1.3 m by the year 2100 in New York City, translating to average rates of 7–13 mm/yr—substantially faster than the current rate of 4 mm/yr based on monthly mean sea level data from 1911 to 2014 [*National Oceanic and Atmospheric Administration*, 2015]. Recent work also suggests that climate change will increase the frequency of the most intense hurricanes and tropical storms [e.g., *Knutson et al.*, 2010; *Emanuel*, 2013]. The cumulative impacts of rising sea level and more frequent, more intense storms will influence the behavior of barrier islands in the future [e.g., *Leatherman*, 1983; *Titus et al.*, 1991; *Sherwood et al.*, 2014; *Durán Vinent and Moore*, 2015].

In recent decades, significant progress has been made in understanding the geological development of barrier islands and the important role of overwash in their evolution. Field-based studies have captured measurements of overwash geometry, volume, and spatial configuration [e.g., *Morton and Sallenger*, 2003; *Donnelly and Sallenger*, 2007; *Carruthers et al.*, 2013; *Williams*, 2015; *Shaw et al.*, 2015; *Lazarus and Armstrong*, 2015]. Deposition of overwash sediment can occur as a result of wave runup exceeding the dune crest (classified as runup overwash) or as a result of the mean water level (tides plus storm surge) exceeding

the dune crest (classified as inundation overwash) [*Sallenger*, 2000]. Runup overwash typically produces overwash fans arising from confined flow, whereas inundation overwash generally results in sheetwash deposits arising from laterally unconfined flow. Back-beach morphology, vegetation, and development also affect the shape and characteristics of overwash deposition [*Donnelly et al*., 2006]. *Sallenger et al*. [2001, 2003] and *Stockdon et al*. [2002, 2009] improved upon the accuracy of ground-based methods for characterizing and measuring overwash by introducing the use of lidar to resolve beach-change signals. Early work by *White and Wang* [2003] used small-scale lidar-derived digital elevation models to determine spatial patterns of coastal volumetric change. They identified a statistically significant difference in net volumetric change over a 4 year period in regions of the beach categorized as developed, undeveloped, or nourished. Additionally, tools have been developed to model and predict erosion in response to the devastation caused by recent storms such as Hurricanes Katrina and Sandy. These include, but are not limited to, process-based models of waves and sediment transport [e.g., *Roelvink et al*., 2009; *Palmsten and Holman*, 2012] and statistical Bayesian modeling approaches [e.g., *Plant and Stockdon*, 2012].

Previous studies address the impacts of anthropogenic structures and development on overwash delivery from a purely qualitative perspective, however, and these impacts have yet to be quantified. Not only is the presence of human development on islands increasingly common but there is a strong coupling between the socioeconomic value placed on barrier islands and the morphologic evolution of islands themselves [e.g., *Werner and McNamara*, 2007; *McNamara and Werner*, 2008a, 2008b; *McNamara and Keeler*, 2013; *Jin et al*., 2013; *Lazarus*, 2014]. Anthropogenic influence and associated feedbacks have long been recognized for their impact in other natural systems. For example, anthropogenic modification of river systems interrupts the hydrological cycle and causes magnified flood stages [*Criss and Shock*, 2001], overfishing of the world's fish supply leads to loss of biodiversity [*Jackson et al*., 2001], and increases in wildfire severity have been linked to fire prevention practices, which lead to excess fuel available for burning [*Schoennagel et al*., 2004]. However, our understanding of the feedbacks associated with human alteration of barrier islands is in its early stages.

Because overwash supplies sediment to the subaerial island and is the mechanism by which islands migrate landward and maintain elevation above sea level, loss or reduction of sediment delivery to the island interior may ultimately lead to island narrowing and drowning, a phenomenon recognized from the results of numerical modeling of island behavior [*Magliocca et al*., 2011]. Many barrier island evolution models incorporate overwash flux as an adjustable parameter [e.g., *Wolinsky and Murray*, 2009; *Lorenzo-Trueba and Ashton*, 2014; *Walters et al*., 2014]; however, overwash flux is poorly constrained (especially as it relates to developed shorelines) and direct measurements of overwash have yet to be used to parameterize overwash flux in models of island evolution.

Here using lidar-based surveys of topography collected before and after Hurricane Sandy along a barrier island in New Jersey, USA, we quantify the impact of anthropogenic structures on the landward extent and volume of overwash deposition relative to a nearby natural area. We then use these results to parameterize a model of barrier island evolution (from *Lorenzo-Trueba and Ashton* [2014]) to demonstrate the likely effect of anthropogenically generated differences in overwash delivery on long-term barrier evolution.

2. Storm Statistics and Study Area

Hurricane Sandy made landfall northeast of Atlantic City, New Jersey, on 29 October 2012 [*Blake et al*., 2013]. Storm surge coupled with spring tides brought water levels to more than 1 m above average for a full day [*National Oceanic and Atmospheric Administration*, 2013b] and led to record-breaking high water levels throughout New Jersey. At The Battery, NY, and Atlantic City, NJ, maximum water levels recorded by tide gauges (effects of storm surge only) reached 3.5 and 2.0 m mean sea level (msl) (2.1 m North American Vertical Datum of 1988 (NAVD88); NJ conversion from *National Oceanic and Atmospheric Administration* [2013a]), respectively [*NOAA*, 2013b]. Oceanfront flood elevations determined from high water marks collected from the interior of homes (including storm surge and wave setup) were 4.6 and 4.2 m msl (4.7 and 4.3 m NAVD88) in Bay Head and Mantaloking, NJ, respectively, whereas high water marks on the exterior of homes and wrack line measurements (both of which include storm surge, wave setup, and wave runup) across the same region averaged 5.4 m msl (5.5 m NAVD88) [*Irish et al*., 2013]. Maximum sustained wind speeds of 130 km/h with gusts up to 145 km/h were recorded in New York and New Jersey. The overall

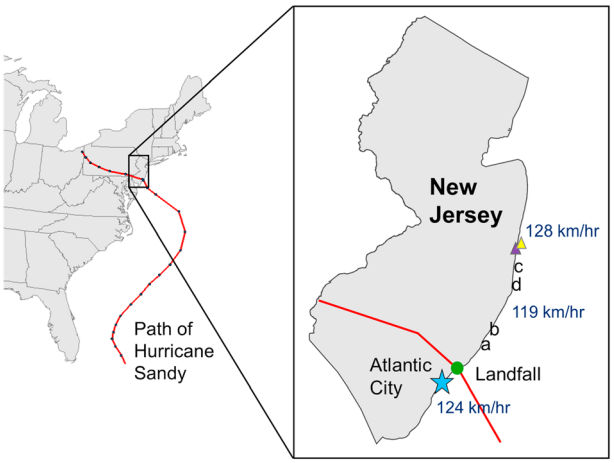

Figure 1. Path of Hurricane Sandy and location of study sites relative to the storm's landfall. Maximum wind speeds (km/h) along the coast are depicted in dark blue. (a–d) Post-Sandy images shown in Figure 2. Purple and yellow triangles depict Mantaloking and Bay Head, NJ, respectively.

minimum central pressure reached 940 mb just hours prior to landfall. Preliminary reports estimate that the storm caused nearly $50 billion in damage within the U. S. [*Blake et al.*, 2013].

We analyze overwash deposition in four areas within a 60 km alongshore reach north of Sandy's landfall, encompassing three categories of environments: (1) a natural environment, which is relatively undisturbed by human influence; (2) a residential environment; and (3) a commercial environment (Figures 1 and 2). A 1.2 km long alongshore reach within the Edwin B. Forsyth Wildlife Refuge serves as the "natural environment" study site. The "residential environment" consists of two regions for comparison to reduce biases introduced as a result of the relative alongshore location of the environments. The first is within Long Beach Township, and the second is roughly 50 km north at Normandy Beach. Both residential areas are characterized by the presence of family-size homes (alongshore frontage = 55%) built on piling foundations amidst shore-perpendicular roads, the majority of which (greater than 75%) terminate within 60 m of the shoreline. The boardwalk of Seaside Heights, NJ, serves as the "commercial environment" and is characterized by the presence of a continuous boardwalk (elevation ~4.5 m) fronting contiguous commercial buildings (alongshore frontage = 92%) built on slab foundations behind which shore-perpendicular roads terminate more than 60 m from the shoreline (Figures 1 and 2). The density of shore-perpendicular roads is comparable between the residential and commercial environments at ~20 roads/km (residential area b: 20–26 roads/km, residential area c: 15–20 roads/km, and commercial area d: 20–24 roads/km). The tidal range at all sites is approximately 1.8 m [*NOAA*, 2013b] with prevailing winds from the northwest. Average prestorm profile elevation ranges from 2.5 m to 4.5 m across the environments (Figure 3), and much of this variation is attributable to differences in development. High water marks indicating storm surge flood levels (surge and tides only, excluding the effects of waves) at the north and

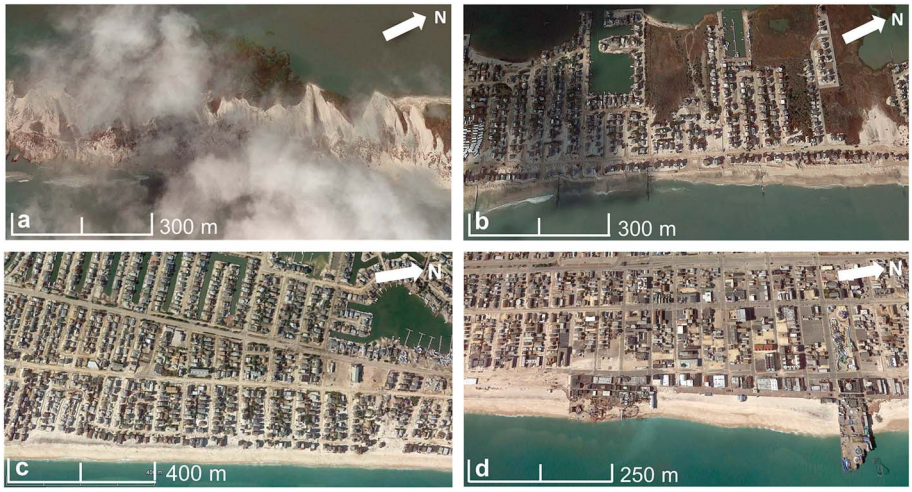

Figure 2. Post-Hurricane Sandy aerial images of each study site (refer to Figure 1 for relative locations): (a) the natural area site within the Edwin B. Forsythe National Wildlife Refuge, (b) residential site in Long Beach Township, (c) residential site at Normandy Beach, and (d) commercial site at the Seaside Heights boardwalk. Imagery source: Google Earth, 3 November 2012.

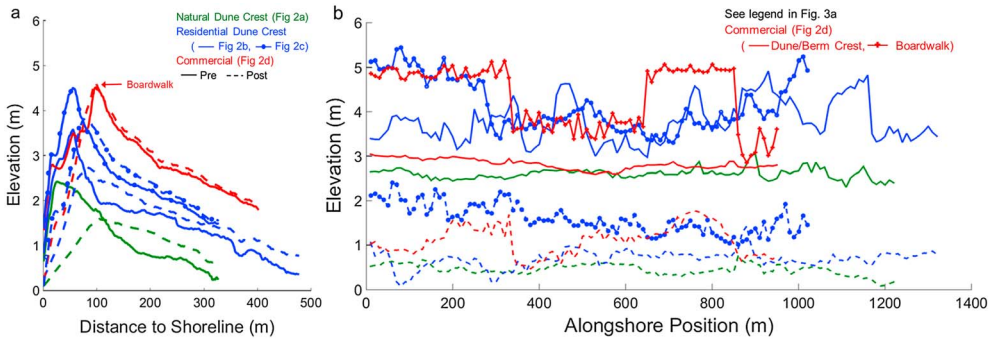

Figure 3. (a) Average prestorm and poststorm elevation profiles (based on 90–130 profiles for each area; see Table 2) for the specified environment showing the degree of change in erosional patterns shoreward of the dune/berm crest (or boardwalk) as well as change in elevation and deposition thickness beyond the dune. (b) Dune/berm elevation prestorm and poststorm illustrating the degree of erosion relative to the alongshore position. Elevations for both the dune/berm crest and boardwalk are shown in the commercial environment for reference.

south ends of our study area were within 0.25 m, at 2.65 m, and 2.40 m (NAVD88; hereafter, all elevations are reported relative to datum NAVD88), respectively as reported by *McCallum et al.* [2013], and maximum wind speeds across the study area were within a 10 km/h range (Figure 1) [*Blake et al.*, 2013]. The close proximity of our sites, the large size of this "super storm" relative to the length of our study area, and the similarity of both high water mark elevations and wind speeds allow us to assume that observed differences in overwash extent and volume across the sites may be related to differences in development rather than storm characteristics.

3. Methods and Results

3.1. Overwash Analysis

3.1.1. Calculation of Overwash Extent and Volume

We quantify the impact of anthropogenic development on the delivery of overwash sediment to the island interior by targeting two related parameters: (1) the landward extent of overwash deposition and (2) the volume of overwash sediment. For the purpose of this study, we define the landward overwash extent as the distance in meters from the prestorm mean high water (MHW) shoreline to the landward most reach of overwash deposition (measured perpendicular to the shoreline). Volume of deposition is measured as the total quantity of sediment deposited beyond the prestorm dune crest. The prestorm MHW shoreline is defined as the 0.7 m contour line. We use lidar first-return surveys collected by the U.S. Geological Survey [*Wright et al.*, 2014] to generate pre-Hurricane Sandy and post-Hurricane Sandy elevation profiles that allow us to measure variability in three dimensions. Point spacing and system error measurements are summarized in Table 1. These surveys are supplemented with field mapping and visual observations of prestorm and storm-derived sedimentologic deposits (see supporting information).

To prepare both prestorm and poststorm data sets we use an adaptive triangular irregular network densification algorithm within ADPAT 1.0 (U.S. Geological Survey developed software [*Zhang and Cui*, 2007]) to remove buildings and vegetation; we use orthorectified aerial photos to verify that only bare-Earth points are retained. Quick Terrain Modeler uses a nearest neighbor interpolation method to create prestorm and poststorm surface models utilizing the data set point spacing to define the underlying grid spacing and optimize resolution. We difference the two surface models to create a prestorm to poststorm elevation change model (Figure 4). Edge error induced by nearest neighbor interpolation reduces and in some cases eliminates areas of no data (which appear black in Figure 4), where buildings and vegetation points are removed. Using all three models, we then extract relevant parameters for quantification. The prestorm MHW shoreline serves as a baseline for measurements collected along cross-shore transects (perpendicular

Table 1. Lidar Metadata

Location	Storm	Collected by	Collection Date	Vertical/Horizontal Accuracy	Point Spacing
Ocean County, NJ	Hurricane Sandy—Before	USGS—EAARL-B	26 Oct 12	20 cm/1 m	0.5–1.6 m
	Hurricane Sandy—After	USGS—EAARL-B	01–05 Nov 12	20 cm/1 m	0.5–1.6 m

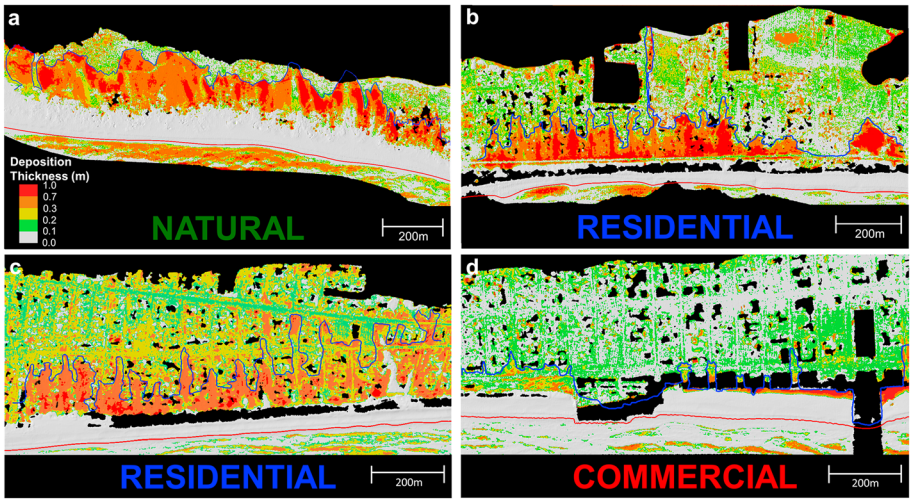

Figure 4. Elevation change models depicting the thickness of sediment deposition and the digitized extent of overwash shown in blue. The mean high water shoreline is shown in red. (a) Natural environment, (b and c) residential environments, and (d) commercial environment. Infrastructure and vegetation data points are removed (indicated by black).

to the shoreline) placed at 10 m alongshore intervals (Figure 5). The number of transects measured and the cross-shore lengths of transects for each environment are summarized in Table 2. Transects reaching into the back-barrier bay are truncated to reflect only subaerial data.

To determine the landward extent of overwash deposition at each transect we use the lidar-derived elevation change model in combination with aerial imagery. The landward extent of overwash deposition in the natural environment is easily manually digitized using imagery by visually comparing the prestorm and poststorm images to identify the seaward edge of fresh overwash deposits. However, given that manually digitizing from aerial imagery in developed areas is substantially more complex (because limited color contrast makes it difficult to distinguish between overwash sand and preexisting sand in driveways and yards), we use the overwash extent digitized from imagery in the natural environment to iteratively determine an elevation threshold (through repeated comparison and adjustment until arriving at a match between the digitized extent derived from aerial imagery and the extent generated by digitizing the binary boundary), which represents overwash within the lidar elevation change model (Figure 6). We then apply this threshold value to the lidar elevation change models for the residential and commercial areas so that we can clearly see and then manually digitize the landward overwash extent in these more complex environments. A modified use of the Digital Shoreline Analysis System [*Thieler et al.*, 2009] calculates the distance from the shoreline to the maximum extent

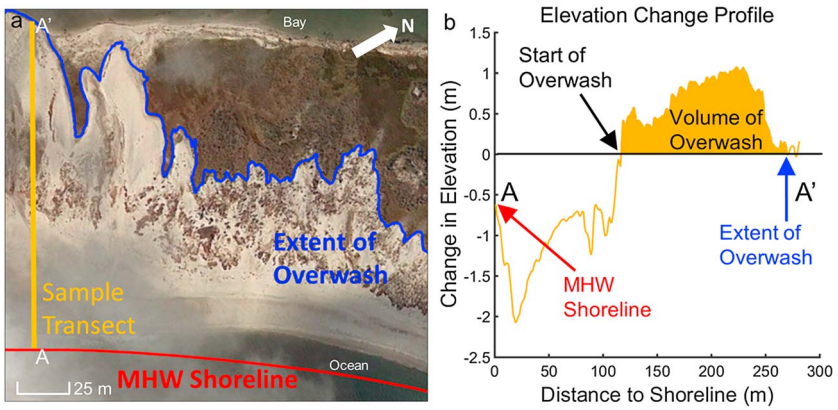

Figure 5. (a) Depiction of the prestorm mean high water (MHW) shoreline, post-Sandy overwash extent, and sample cross-shore transect. (b) Annotated change profile along a cross-shore transect from A to A' (location shown in Figure 5a) measured from the shoreline showing the start, extent, and volume of an overwash deposit.

Table 2. Summary of Number and Length of Transect by Environment

Location (Environment)	Number of Transects	Maximum Length (m)
Edwin B. Forsythe (natural)	122	325
Long Beach Township (residential)	132	425
Normandy Beach (residential)	99	425
Seaside Heights (commercial)	92	400

of overwash deposition along each transect. For ease of comparison, we represent overwash extent both dimensionally (E_{ow}; absolute extent of overwash in meters) and in a nondimensionalized form:

$$E^*_{ow} = \frac{E_{ow}}{W_{BI}} \quad (1)$$

where E^*_{ow} is the nondimensionalized extent of overwash and W_{BI} is the initial cross-shore width of the barrier island in meters.

To calculate the volume of overwash deposition along each transect, we compute the area under the elevation change profile and represent these volumes as width-averaged quantities in units of m^3/m. The point at which deposition begins is defined as the location where the elevation change becomes positive; deposition ends at the limit of extent of overwash deposition (Figure 5). We define characteristic overwash deposition geometries for each environment by averaging profiles across each study area (Figure 7).

3.1.2. Error Analysis

Error in lidar data is attributed to a combination of four components: lidar system measurement error (related to component calibration), interpolation error (introduced when creating surface models and increases with increased point spacing), horizontal displacement (caused by GPS positioning error), and surveyor (or human interpretation) error [*Hodgson and Bresnahan*, 2004]. *Sallenger et al*. [2003] found that they could resolve beach-change signals in lidar surveys with a vertical precision of ±15 cm. However, when detecting change across temporal scales, relative lidar system measurement error (or the vertical survey offset created by system measurement error) is the most important error to address [*Zhang et al*., 2005]. Thus, we compare 20 control points between the prestorm and poststorm first-return surveys to determine if vertical offset

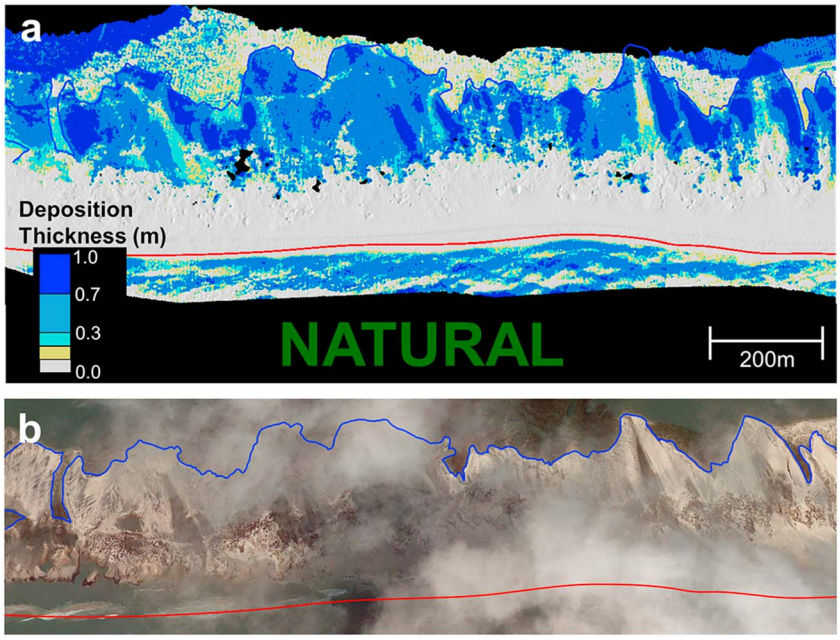

Figure 6. Illustration of the elevation threshold used to digitize the extent of overwash deposition. (a) The elevation change model and (b) the corresponding aerial imagery demonstrate the fit of the resolved threshold as determined in the natural area for application in the residential and commercial areas.

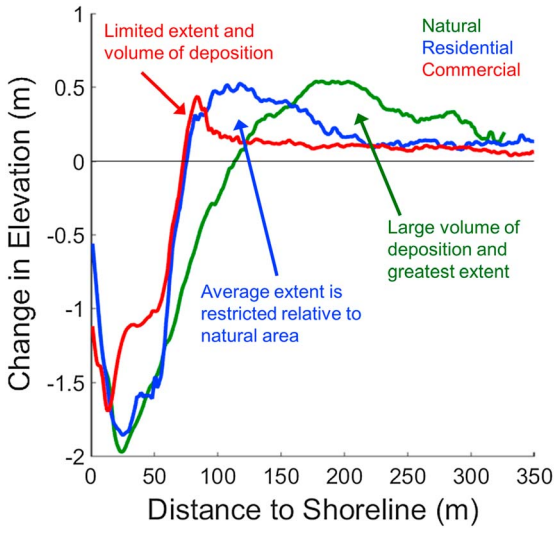

Figure 7. Average change profiles for each environment show patterns of erosion and overwash distribution. In the natural environment, erosion extends farther landward, but overwash deposits are greater in volume and landward extent relative to developed areas.

created by system error is a factor. We use building corners for most of our control points, as they are easily identifiable and unlikely to be altered by the storm. Direct comparison of the control points for each survey yields an R^2 correlation of 0.99 with an absolute mean error of less than 5 cm. We therefore consider relative offset error to be negligible.

To quantify errors associated with interpolation we removed 1000 points prior to interpolation for comparison to postinterpolation points. The resulting ~5 cm of vertical error is likely an overestimate as removing 1000 points from the data series increases the distance between points (thereby introducing error). Additional details of the error analysis appear in the Supporting Information.

3.1.3. Characteristics of Overwash Deposition

Prior to Hurricane Sandy, the dune crest in the natural area reached an average elevation of 2.5 m and was located approximately 20 m landward of the shoreline. Vegetation consisted of mature dune grasses backed by marsh, and previous overwash deposits are clearly visible in prestorm satellite imagery. To ensure that only the extents of newly deposited overwash fans were analyzed, we completed a prestorm and poststorm image comparison.

Dunes in the natural environment were uniformly reduced by approximately 2.0 m in elevation during Hurricane Sandy (Figure 3). Visual inspection of aerial images indicates deposition consistent with laterally unconfined flow (i.e., inundation overwash). Landward overwash extent ranged from 188 to 309 m (average = 252 m) and reached the back-barrier bay in 28% of profiles. The volume deposited ranged from 23 to 125 m^3/m (Figures 8 and 9 and Table 3). Volume of sediment deposited into the back-barrier bay, however, is not captured in measurements, leading to a likely underprediction of both landward overwash extent and volume of deposition in the natural environment.

In the two residential areas, prestorm dune crests averaged 3.5–4.5 m in elevation and beach access points were only slightly lower than average at 3 m and higher in elevation. The beach and dune were consistently overwashed alongshore in both residential environments, resulting in a substantial decrease in dune height of ~2–3 m everywhere alongshore (Figure 3). Areas where overwash deposition occurred beyond the dune

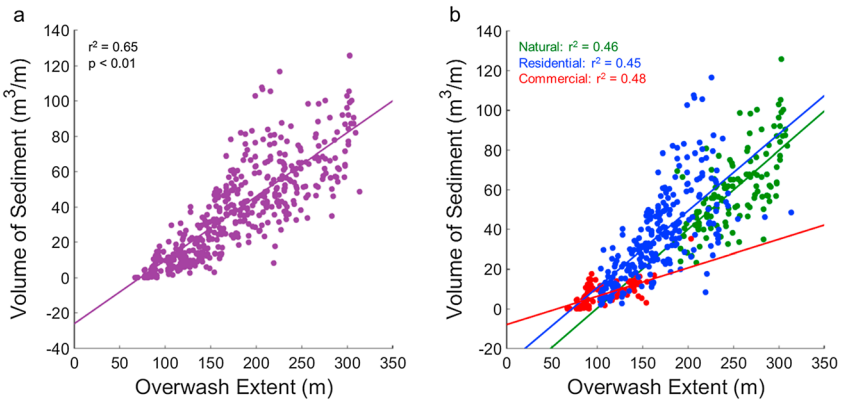

Figure 8. (a) The linear dependence of overwash volume on overwash extent, accounting for the offset between the mean high water shoreline and the cross-shore location where overwash begins. (b) Separating by environment, the relationship remains linear.

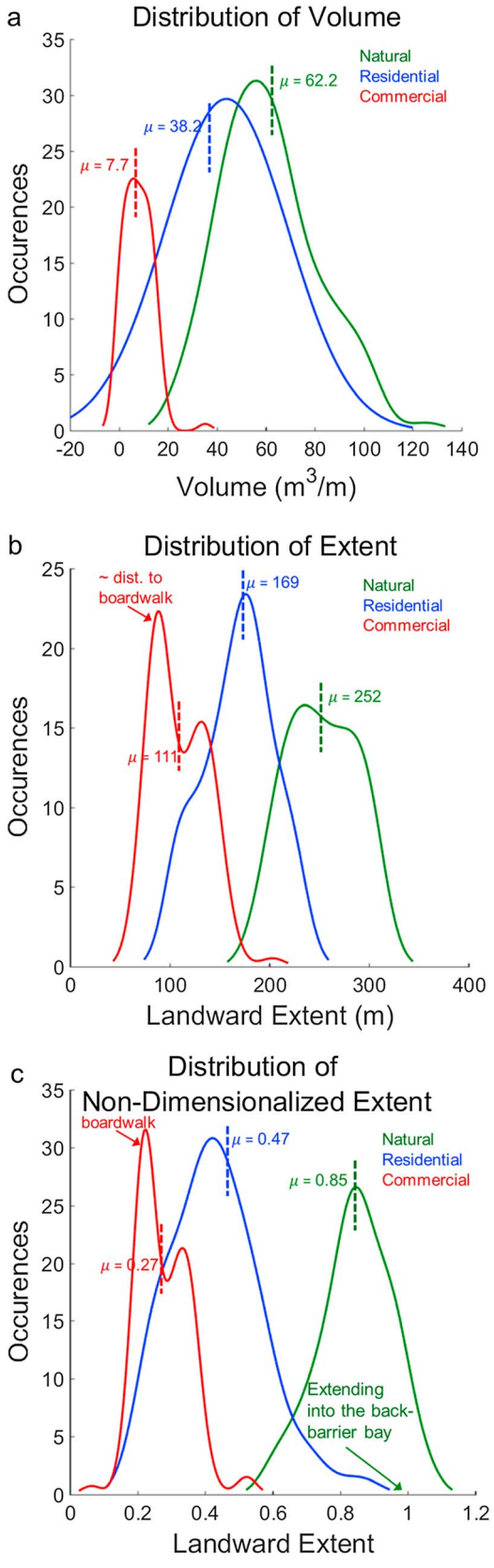

crest as confined, channelized flow (primarily along roads) tended to correspond with locations where overwash penetration and volume were greatest. The average landward overwash extent in the residential environments is 169 m, and volumes range from 2 to 117 m^3/m (Figures 8 and 9 and Table 3).

Likely because the dune/berm crest was narrow and low (~3 m in elevation) in the commercial area, extensive damage occurred to the boardwalk which sits at 4.5 m in elevation, 75–100 m from the shoreline. Regions of confined flow occurred along this section of beach but were less common than in the residential area (fewer channels per kilometer). The average landward extent of overwash deposition in the commercial environments was 111 m, and overwash volume ranges from 0 to 35 m^3/m (Figures 8 and 9 and Table 3).

3.1.4. Distribution of Overwash

Where overwash flow was uninhibited by anthropogenic structures (i.e., in the natural environment), no signs of channelized flow were visible, whereas although dunes were uniformly eroded, channelized, confined overwash events were prevalent in the residential and commercial environments. Combining measurements from all environments, we compared the landward overwash extent and volume of deposition The resulting statistically significant linear relationship ($R^2 = 0.68, p < 0.01$) (Figure 8a) can be described as

$$V_{ow} = K \times E_{ow} - A \quad (2)$$

where V_{ow} is the volume of overwash, K is a coefficient, and A is a constant which accounts for offset between the shoreline and the cross-shore location where overwash begins. Considering all environments together, we find the coefficient (K) to be 0.36. The relationships found here are nearly identical to those defined by *Overbeck et al.* [2015], who investigated overwash deposition of Fire Island, New York following Hurricane Sandy and found the relationship between overwash and extent and volume to be linear with coefficients (K) ranging from 0.35 to 0.41 (although they do not differentiate between developed and undeveloped areas). When we repeat the same analysis for each environment, the relationships remain linear and statistically significant ($p < 0.01$ for all environments), but values of K and A differ, most markedly for the commercial area where the coefficient (K) is 0.14 (Figure 8b and Table 4).

Figure 9. Distribution of (a) overwash volume, (b) landward extent of overwash, and (c) nondimensionalized extent of overwash. Overwash deposition is greatest in volume and extent in the natural area. Overwash volumes delivered to the residential and commercial environments are 40% and 90% of that delivered to the natural area, respectively.

Table 3. Overwash Characteristics by Environment

Environment	No. of Transects	E_{OW} Range (m)	Average E_{OW} (m)	Average E^*_{OW}	V_{OW} Range (m^3/m)	Average V_{OW} (m^3/m)
Natural	122	188–309	252.2	0.85	23.3–125.7	62.2
Residential	231	103–271	169.0	0.47	2.1–116.7	38.1
Commercial	92	25–203	108.1	0.27	0–35.1	7.7

When anthropogenic factors are introduced, both the volume and landward extent of overwash deposition decrease with increasing waterfront development, as defined within our study. The average volume of sediment delivered to the residential and commercial environments is reduced to just 60% and 10% of that delivered to the natural environment, respectively. Similarly, the average extent of overwash in the natural environment was more than 2.25 times greater than in the commercial environment. Although the effect on overwash delivery of a boardwalk in association with contiguous commercial buildings has not previously been quantified, the 90% reduction in overwash delivery in the commercial area relative to the natural area is expected, given that the boardwalk sits at an elevation of 4.5 m. The buildings landward of the boardwalk sustained only minimal damage, whereas the boardwalk was nearly entirely destroyed, suggesting that the boardwalk alone would have been a less effective obstacle and that the presence of contiguous, slab foundation buildings contributed to the reduction in overwash delivery. The range of values for both extent and volume (Figure 9) was greatest for the residential environment (shown in both dimensional and nondimensional terms). Only in the natural environment did overwash extend into the back-barrier bay (i.e., extent >1 in nondimensionalized terms; Figure 9c).

We can additionally consider the mass balance for each environment. An important consideration here is that our measurements of the system are not closed because topographic lidar data limit the analysis to the subaerial landscape (and thus constrain an analysis of how much sand is lost). We calculated the mass balance as the difference between the total volume of sand deposited by overwash and the total volume of subaerial sand eroded, as measured from the shoreline to the bay within an environment. Although sand delivered to, and captured by, the bay in the natural environment (and the offshore in all environments) could not be accounted for, and although the patterns of deposition were most different between the natural and commercial environments, the mass balance in these two environments was similar: their volumes were within 15% of each other, at an average sand loss of 5.3 m^3/m and 4.6 m^3/m for the natural and commercial environments, respectively. By comparison, the residential area lost an average of 2.9 m^3/m of sand, although this number is likely artificially low because we were unable to account for large amounts of sand eroded from beneath the piling foundations of the many homes located within the zone of erosion (Figure 4), a phenomenon observed in poststorm photographs.

The results of our analysis suggest the following scaling relationships for the volume and extent of overwash deposition as a function of the type of anthropogenic environment (assuming similar bathymetry and back-barrier elevation), for future use in analytic and exploratory models of barrier island processes:

	Natural	**Residential**	**Commercial**
Volume	$V_{ow,\ N}=V_{ow,N}$	$V_{ow,\ R}=0.6\times V_{ow,N}$	$V_{ow,\ C}=0.1\times V_{ow,N}$
Landward Extent (m)	$E_{ow,\ N}=E_{ow,N}$	$E_{ow,\ R}=0.7\times\ E_{ow,N}$	$E_{ow,\ C}=0.4\times\ E_{ow,N}$

(3)

These equations present generalized relationships based on the type of environment as defined in section 2. If using these equations to consider overwash delivery in other locations, many factors must be carefully considered and accounted for: the type of structures, road density, road termination distance, presence or absence and elevation of a boardwalk, and dune height relative to the sites considered here.

Table 4. Overwash Relationship Variables[a]

Environment	K	A
Combined	0.36	−26
Natural	0.40	−39
Residential	0.39	−27
Commercial	0.14	−8

[a]K—relationship coefficient, A—shoreline to overwash offset constant.

3.1.5. The Role of Prestorm Dune Height

Because overwash deposition can be a function of both infrastructure and dune height (factors which are linked and difficult to differentiate), we explore the relationship between prestorm dune height

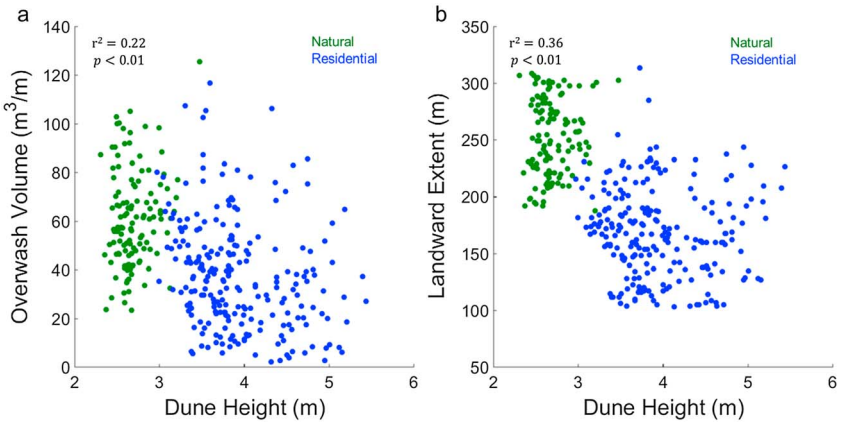

Figure 10. Role of prestorm dune height on overwash deposition volume and landward extent of overwash. Each data point represents one transect within the designated environment. Prestorm dune height and (a) overwash volume and (b) landward extent of overwash are both negatively, but weakly, correlated.

and overwash extent and volume (Figure 10). We find prestorm dune height to be weakly correlated with overwash volume and extent ($R^2 = 0.22$ and $R^2 = 0.36$, respectively). Although this correlation is statistically significant ($p < 0.01$) (Figure 10), dune height is not strongly predictive of overwash deposition in this study, likely because all of the dunes (and the dune/berm in the commercial area) appear to have been overtopped by the combination of storm surge, wave setup, and wave runup, regardless of their initial height. Widespread and prolonged overtopping (likely due to the high intensity and sustained duration of Hurricane Sandy) is consistent with two lines of evidence: the substantial reduction in dune height of 2–3 m across the entire alongshore extent of all environments (Figure 3) and the oceanfront exterior and wrack line high water marks reported by *Irish et al*. [2013], which average 5.4 m (and include the effects of wave setup and wave runup), nearly a meter above the highest average dune height of 4.5 m in any of our study areas (Figure 3a) and 0.25 m above the highest of the individual dune peaks (Figure 3b). Therefore, although we cannot completely separate the effect of buildings and dunes on overwash delivery and thus rule out the possibility that overwash was less persistent or less energetic where dunes were higher, the large-scale, prolonged overtopping of dunes throughout the study area and the lack of predictive strength of the relationship between prestorm dune height and overwash extent and volume suggest that structures play a role in reducing overwash deposition in all developed, residential and commercial, areas we investigated.

3.2. Long-Term Impacts on Barrier Island Evolution

We use an exploratory morphodynamic barrier island evolution model, introduced by *Lorenzo-Trueba and Ashton* [2014], to investigate modes of island behavior under a variety of conditions. This model considers a barrier island cross section through an idealized geometric configuration and uses a system of equations to determine long-term (decades to centuries to millennia) island tendencies. Three change components (passive flooding due to sea level rise, shoreface fluxes, and overwash) determine the evolution of the barrier system, which is fully resolved by the shoreline toe, the shoreline, the back-barrier, the barrier height, and the rate of change of the back-barrier height. This system of equations is numerically solved to examine coupled, nonsteady state behaviors that include dynamic equilibrium, height drowning, and width drowning. Height drowning in this model occurs when sediment fluxes due to overwash are insufficient to maintain island elevation relative to rising sea level. Width drowning occurs when sediment flux to the back-barrier is insufficient to maintain island geometry during landward migration (Figure 11).

We use this model to investigate the long-term impact of decreases in overwash delivery on island evolution caused by development. To provide context for considering implications across barrier island systems broadly, we apply generic island characteristics similar to those used by *Lorenzo-Trueba and Ashton* [2014] (Table 5), in conjunction with the empirically derived scaling relationships for overwash flux ($Q_{ow,\ max}$) we present at the end of section 3.1.4. *Lorenzo-Trueba and Ashton* [2014] capture impacts of storm frequency

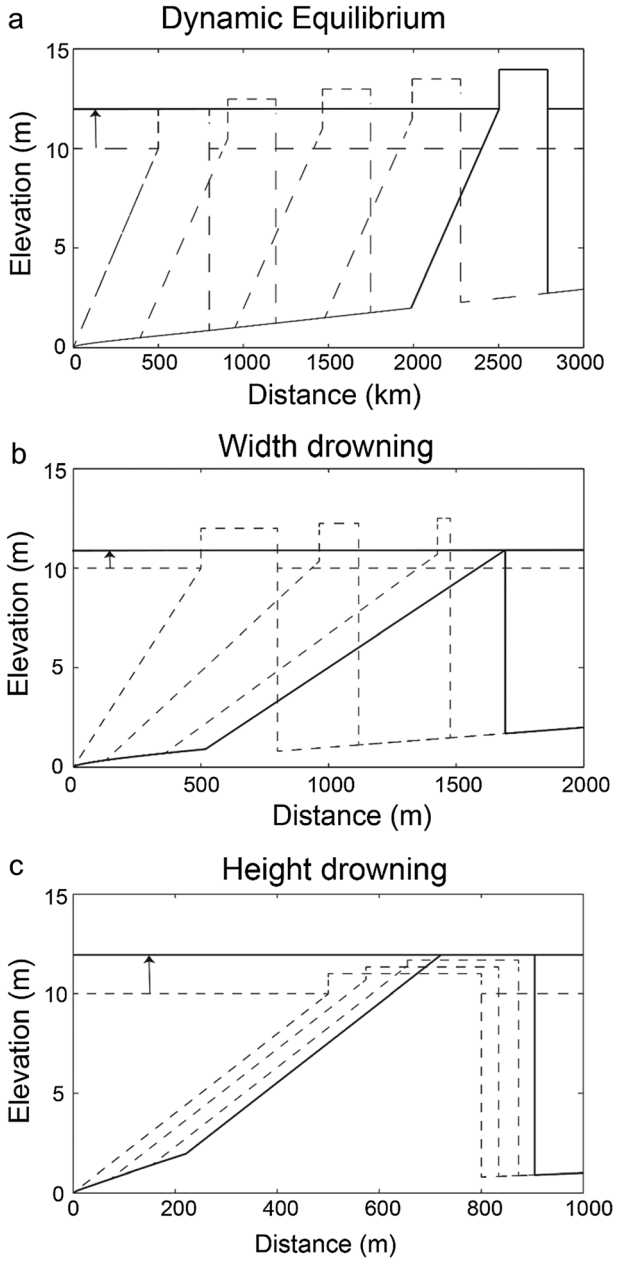

Figure 11. Island states as described in *Lorenzo-Trueba and Ashton* [2014]. (a) Dynamic equilibrium, (b) width drowning, and (c) height drowning.

and magnitude as well as potential anthropogenic effects in a single term, $Q_{ow,\ max}$, which represents the maximum annual volume of overwash delivered by all storms. *Lorenzo-Trueba and Ashton* [2014] explore values for $Q_{ow,\ max}$ of 0–100 m^3/m/yr. For consistency with this previous work, we set $Q_{ow,\ max}$ to 30 m^3/m/yr to represent the natural environment. This value is equal to 50% of the volume of overwash deposition we calculated for this environment. We chose this midrange value, given that Hurricane Sandy was an anomalously large storm and our goal is to explore scenarios more representative of typical conditions. We then apply equation (3), yielding scaled $Q_{ow,\ max}$ values of 18 and 3 m^3/m/yr for the residential and commercial environments, respectively. Simulations suggest that the effect of decreasing overwash flux to the back-barrier (with scaled values for the different environments represented by green, blue, and red lines for comparison in Figure 12) changes the long-term behavior of the island. At significantly high rates of SLR (>8 mm/yr) and deeper back-barrier depths (>9 m), the natural environment responds by maintaining dynamic equilibrium (Figure 12c, vertical green line). In contrast, decreases in overwash flux associated with increasing density of development lead to width drowning in the residential environment and height drowning in the commercial environment (Figure 12c, vertical blue and red lines). It should be noted that Figure 12c represents a worse-case scenario illustrating that the risk of drowning is greatly increased as the rate of SLR increases and as the depth of the

Table 5. Input Parameters Used in Figure 12

Parameter	Symbol	Units	Value
Shoreface response rate	K	m^3/m/yr	10,000
Equilibrium shoreface slope	A	-	0.02
Shoreface toe depth	D_t	m	10
Equilibrium island width	W	m	300
Equilibrium island height	H	m	2
Back barrier bay depth	D_b	m	2, 5, and 9
Sea level rise	Z	mm/yr	0–15
Maximum overwash flux (natural)	$Q_{ow,\ max}$	m^3/m/yr	30
Maximum overwash flux (residential)	$Q_{ow,\ max}$	m^3/m/yr	18
Maximum overwash flux (commercial)	$Q_{ow,\ max}$	m^3/m/yr	3

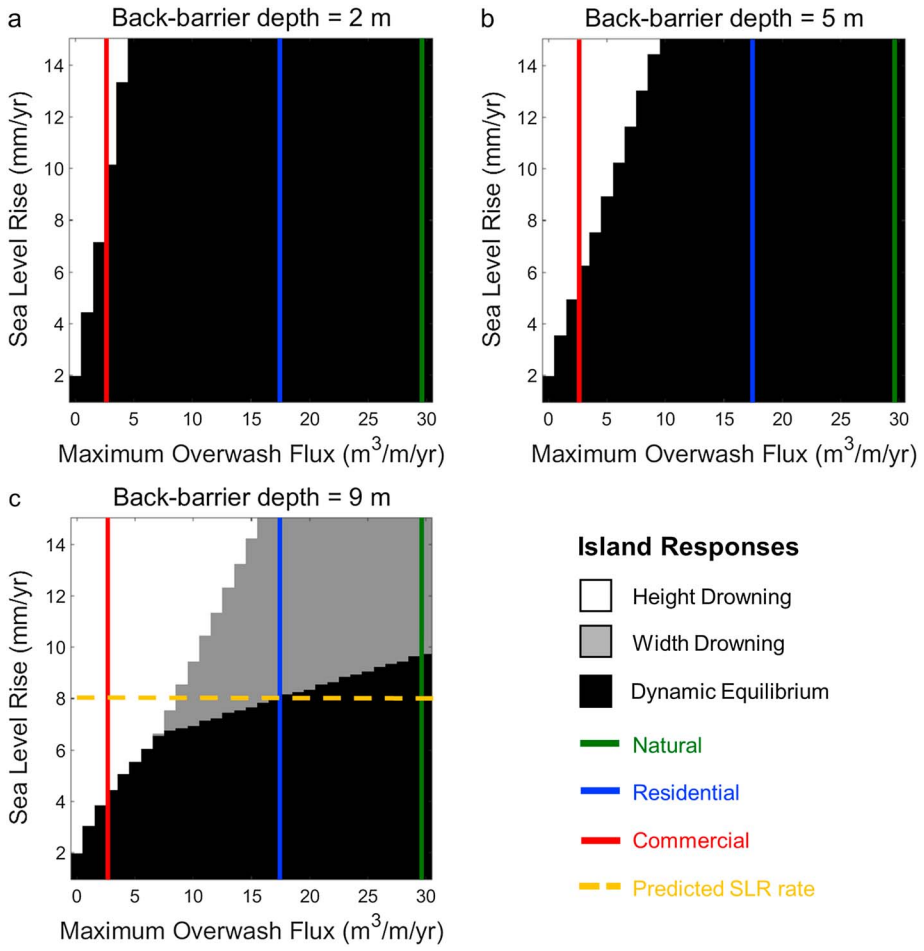

Figure 12. Phase diagrams illustrating the impact of different overwash fluxes (arising from different degrees of filtering by development) on barrier island evolution for a range of sea level rise rates and back-barrier depths of (a) 2 m, (b) 5 m, and (c) 9 m. Red and blue lines denote maximum overwash flux ($Q_{ow,\ max}$) for commercial and residential environments, respectively, scaled relative to a natural environment $Q_{ow,\ max}$ of 30 m^3/m/yr according to relationships presented in section 3.1.4.

back-barrier bay increases. For comparison, the average depths of Barnegat Bay (NJ, USA), Pamlico Sound (NC, USA), and the Chesapeake Bay (MD/VA, USA) are 1, 2, and 6 m, respectively [*Miselis et al.*, 2013; *Urquhart et al.*, 2013].

4. Discussion

The volumes and landward extents of overwash deposition measured in this study are 0–125 m^3/m and 25–310 m, respectively. These values represent both natural and anthropogenic environments and fall within the expected range based on previous estimates. *Carruthers et al.* [2013] compile 30 estimates of overwash fan geometric properties from a number of studies and report landward overwash extents of 13–359 m and volumes of 8–190 m^3/m, respectively. Additionally, the average volume of 62 m^3/m calculated for our natural environment is well in line with that estimated for overwash associated with the Hurricane of 1938 on Long Island, NY, of ~54–80 m^3/m [*Redfield and Miller*, 1955], an environment broadly similar to that studied here.

Our results extend previous work on overwash by demonstrating a linear relationship between overwash extent and volume (Figure 8). Furthermore, our findings demonstrate that as the landward extent of overwash deposition increases, the relationship with overwash volume becomes less tightly constrained and the range of overwash volumes for any given landward overwash extent increases. This latter phenomenon is likely the result of progressive increases in lateral spreading and infiltration which occur as the landward overwash extent increases, a process described in detail by *Donnelly et al.* [2009]. The linear

relationship between overwash volume and overwash extent identified here, in combination with the linear relationship between overwash extent and overwash depth (i.e., height of water over dune) identified by *Mattias et al.* [2014], suggests that overwash volume and overwash depth should also be linearly related. The severe reduction in dune height during Hurricane Sandy (which makes it unclear which dune height to use to calculate overwash depth), and the effect of structures on overwash processes, confound calculations of overwash depth. Although this prevents us from directly addressing the relationship between overwash depth and overwash volume for our study areas, this may be a fruitful line of inquiry for future studies.

Similar to previous studies, which cite roads as likely conduits for channelized overwash deposition [e.g., *Hall and Halsey*, 1991; *Nordstrom*, 1994; *Houser*, 2013], we find a greater frequency of channelized deposits in the residential and commercial environments relative to the natural environment. Analysis of aerial imagery suggests that locations of channelized flow within the developed environments in our study correspond to road locations, strongly suggesting that infrastructure (i.e., roads and parking lots) and building placement can control overwash deposition.

We find that overwash volume and extent are correlated with prestorm dune height, although the correlation is too weak to be predictive. Because dunes throughout our study areas were uniformly and substantially overtopped by overwash processes, it is clear that even the highest of dunes here were not sufficiently high to prevent overwash from occurring during Hurricane Sandy. Further, even though we cannot rule out the possibility that the presence of higher dunes in the residential area contributed to the reduction in overwash delivery, our quantification of the reduction stands as useful, given that residential oceanfront development is nearly always associated with high, usually artificially maintained, dunes.

The volume of overwash deposition varied according to the type of environment, decreasing to 60% and 10% of that delivered to the natural area in the residential environment (a region of family-size homes built on piling foundations amidst shore-perpendicular roads, the majority of which terminate within 60 m of the shoreline) and commercial environment (continuous boardwalk of elevation ~4.5 m fronting contiguous commercial buildings built on slab foundations behind which shore-perpendicular roads terminate more than 60 m from the shoreline, respectively) (see section 2 for additional details). The 60% reduction in overwash volume in the residential areas relative to the natural areas is consistent with the reduction in overwash volume that would be predicted by the relationship between overwash volume and overwash depth recently identified by *Mattias et al.* [2014]. That is, overwash depth in the residential area was likely ~1/2 that of the natural area given water levels across the study area of 5.5 m as per *Irish et al.* [2013] and dune height of ~3.0 m in the natural area versus ~1.5 m in the residential areas. Because much of the deposition occurring in the developed environments amassed in roads as channelized deposition, the relative volumes measured in this study should be considered upper bounds on deposition; humans will undoubtedly move sand back to the beach (i.e., bull doze to clear roads) during clean-up (in our study we used poststorm surveys collected prior to clean-up). Additionally, sand delivered to the back-barrier bay in the natural environment was not captured due to limitations of topographic (in contrast to bathymetric) lidar. These factors imply that the spread between the amount of overwash sediment delivered to the natural and developed environments is likely even greater than our calculations suggest.

The most dramatic reduction in overwash occurred in the commercial area where, despite the record high water levels produced by Hurricane Sandy, overwash extent was limited to the area seaward of the boardwalk along nearly 50% of transects. This suggests that, in the presence of buildings having a substantial alongshore extent, even major storms are unable to supply overwash sediment to the island interior. From this we can infer that smaller, more frequent storms are also unable to supply sediment to the interior of the island, thereby implying that development effectively filters high-frequency events.

Previous modeling studies [*McNamara and Werner*, 2008a; *Magliocca et al.*, 2011] warn of the long-term consequences of filtering high-frequency overwash events arising from protection of infrastructure in the short term (for example, by building a seawall or large artificial dunes), which may lead to barrier narrowing and drowning. Similar filtering of high-frequency events by anthropogenic manipulation is a recognized phenomenon with major consequences in other geomorphic systems such as major rivers and forested areas [e.g., *Criss and Shock*, 2001; *Schoennagel et al.*, 2004]. Ultimately, the filtering of smaller events has historically led to more extreme, more costly events as demonstrated by river discharge management, wildfire prevention and as predicted in coastal economic models by *McNamara and Werner* [2008a].

Our observational and modeling results suggest that increases in the density and extent of development along barrier island coastlines will reduce overwash delivery, maintaining low barrier islands even as sea level rises, ultimately leading to increases in damage to infrastructure and higher costs of recovery following large, overwash-producing events. Our model results also highlight the potentially catastrophic consequences of high-frequency filtering as it relates to the persistence of barrier islands—they suggest that developed barrier islands will tend toward drowning in the long term under anticipated accelerated SLR, whereas natural barriers will be more likely to persist by means of landward migration via frequent overwash. Thus, we can likely expect filtering of high-frequency—and partial filtering of the low-frequency—delivery of overwash to ultimately impact not only barrier island evolution but also coastal management decision-making and policy (e.g., cost of insurance). Results presented here may be useful in considering the filtering capacity of environments having a similar density of buildings and roads relative to our study areas regardless of whether infrastructure present is primarily commercial or residential. Further work exploring the effects of back-barrier bay depth (i.e., accommodation), interactions between barriers and back-barrier marshes [*Walters et al*., 2014], and complex barrier—inlet—back-barrier dynamics [*FitzGerald et al*., 2008] on island response to decreased overwash delivery, as well as the potentially compounding effects of offshore bars and beach slope on alongshore variation in water level [*Cohn et al*., 2014], would potentially broaden the results found here.

5. Conclusions

We analyzed two key parameters—volume of overwash deposition and landward extent of overwash deposition—to quantify anthropogenic controls on the delivery of overwash sediment. By categorizing the section of the New Jersey shoreline immediately north of where Hurricane Sandy made landfall into three distinct environments—natural, residential, and commercial—we were able to directly compare overwash characteristics under similar storm conditions. The volumes of deposition in the residential and commercial environments scaled to 60% and 10%, respectively, of the volume deposited in the natural environment volume. This translates into a reduction of overwash delivery by 40% in the residential areas and 90% in the commercial area. The landward extent of overwash was also substantially reduced with increasing shoreline development: in the commercial area, overwash was completely obstructed along 50% of the alongshore reach. This finding suggests that large anthropogenic structures are highly effective at filtering overwash events.

The scaling relationships offered here provide an empirical framework that can be used to parameterize overwash delivery when modeling barrier island evolution in the presence of infrastructure. Model results suggest that anthropogenic reductions in the flux of overwash sediment reaching island interiors may ultimately lead to island drowning. Although Hurricane Sandy was an extreme, low-frequency event, it serves as a good example of the depositional impacts that can be expected in the future with rising sea levels and the increased frequency of more intense storms.

Acknowledgments

The data for this paper are available at NOAA's Digital Coast Data Repository, Data set: *EAARL-B Coastal Topography*: *Eastern New Jersey*, *Hurricane Sandy*, *2012*: *first surface*. No. 767. We thank the UNC Geological Sciences' Martin Fund and the NSF Geomorphology and Land Use Program (grant EAR 1053151) for funding, and we thank Hilary Stockdon and Rudy Troche for assisting us in acquiring the lidar data. Additional thanks to Tamlin Pavelsky, Antonio B. Rodriguez, A. Brad Murray, Associate Editor Curt Storlazzi, Editor Giovanni Coco, and two anonymous reviewers, whose feedbacks helped to improve this manuscript.

References

Blake, E. S., T. B. Kimberlain, R. J. Berg, J. P. Cangialosi, and J. L. Beven II (2013), Tropical cyclone report: Hurricane Sandy, *Nat. Hurricane Center*, *12*, 1–10.

Carruthers, E. A., D. P. Lane, R. L. Evans, J. P. Donnelly, and A. D. Ashton (2013), Quantifying overwash flux in barrier systems: An example from Martha's Vineyard, Massachusetts, USA, *Mar. Geol.*, *343*, 15–28, doi:10.1016/j.margeo.2013.05.013.

Cohn, N., P. Ruggiero, J. Ortiz, and D. J. Walstra (2014), Investigating the role of complex sandbar morphology on nearshore hydrodynamics, *J. Coastal Res.*, *70*, 53–58, doi:10.2112/SI65-010.1.

Criss, R. E., and E. L. Shock (2001), Flood enhancement through flood control, *Geology*, *29*(10), 875–878, doi:10.1130/0091-7613(2001)029<0875:FETFC>2.0.CO;2.

Donnelly, C., and A. H. Sallenger (2007), Characterization and modeling of washover fans, *Proc. Coastal Sediments'*, *07*, 2061–2073, doi:10.1061/40926(239)162.

Donnelly, C., N. Kraus, and M. Larson (2006), State of knowledge on measurement and modeling of coastal overwash, *J. Coastal Res.*, *22*(4), 965–991, doi:10.2112/04-0431.1.

Donnelly, C., H. Hanson, and M. Larson (2009), A numerical model of coastal overwash, *Proc. ICE-Maritime Eng.*, *162*(3), 105–114, doi:10.1680/maen.2009.162.3.105.

Durán Vinent, O., and L. J. Moore (2015), Barrier island bistability induced by biophysical interactions, *Nat. Clim. Change*, *5*(2), 158–162, doi:10.1038/NCLIMATE2474.

Emanuel, K. A. (2013), Downscaling CMIP5 climate models shows increased tropical cyclone activity over the 21st century, *Proc. Natl. Acad. Sci. U.S.A.*, *110*(30), 12,219–12,224, doi:10.1073/pnas.1301293110.

FitzGerald, D. M., M. S. Fenster, B. A. Argow, and I. V. Buynevich (2008), Coastal impacts due to sea-level rise, *Annu. Rev. Earth Planet. Sci.*, *36*, 601–647.

Hall, M. J., and S. D. Halsey (1991), Comparison of overwash penetration from Hurricane Hugo and pre-storm erosion rates for Myrtle Beach and North Myrtle Beach, South Carolina, USA, *J. Coastal Res.*, *8*, 229–235.

Hodgson, M. E., and P. Bresnahan (2004), Accuracy of airborne lidar-derived elevation, *Photogramm. Eng. Remote Sens.*, *70*(3), 331–339.
Honey, M., and D. Krantz (2007), *Global Trends in Coastal Tourism*, Center on Ecotourism and Sustainable Development, Washington, D. C.
Houser, C. (2013), Alongshore variation in the morphology of coastal dunes: Implications for storm response, *Geomorphology*, *199*, 48–61, doi:10.1016/j.geomorph.2012.10.035.
Irish, J. L., P. J. Lynett, R. Weiss, S. M. Smallegan, and W. Cheng (2013), Buried relic seawall mitigates Hurricane Sandy's impacts, *Coastal Eng.*, *80*, 79–82.
Jackson, J. B., et al. (2001), Historical overfishing and the recent collapse of coastal ecosystems, *Science*, *293*(5530), 629–637, doi:10.1126/science.1059199.
Jin, D., A. D. Ashton, and P. Hoagland (2013), Optimal responses to shoreline changes: An integrated economic and geological model with application to curved coasts, *Nat. Resour. Model.*, *26*(4), 572–604, doi:10.1111/nrm.12014.
Knutson, T. R., J. L. McBride, J. Chan, K. Emanuel, G. Holland, C. Landsea, I. Held, J. P. Kossin, A. K. Srivastava, and M. Sugi (2010), Tropical cyclones and climate change, *Nat. Geosci.*, *3*(3), 157–163, doi:10.1038/ngeo779.
Kopp, R. E., R. M. Horton, C. M. Little, J. X. Mitrovica, M. Oppenheimer, D. J. Rasmussen, B. H. Strauss, and C. Tebaldi (2014), Probabilistic 21st and 22nd century sea-level projections at a global network of tide-gauge sites, *Earth's Future*, *2*(8), 383–406, doi:10.1002/2014EF000239.
Lazarus, E. D. (2014), Threshold effects of hazard mitigation in coastal human–environmental systems, *Earth Surf. Dyn.*, *2*(1), 35–45, doi:10.5194/esurf-2-35-2014.
Lazarus, E. D., and S. Armstrong (2015), Self-organized pattern formation in coastal barrier washover deposits, *Geology*, *43*(4), 363–366, doi:10.1130/G36329.1.
Leatherman, S. P. (1983), Barrier dynamics and landward migration with Holocene sea-level rise, *Nature*, *301*, 15–17, doi:10.1038/301415a0.
Lorenzo-Trueba, J., and A. D. Ashton (2014), Rollover, drowning, and discontinuous retreat: Distinct modes of barrier response to sea-level rise arising from a simple morphodynamic model, *J. Geophys. Res. Earth Surf.*, *119*, 779–801, doi:10.1002/2013JF002941.
Magliocca, N. R., D. E. McNamara, and A. B. Murray (2011), Long-term, large-scale morphodynamic effects of artificial dune construction along a barrier island coastline, *J. Coastal Res.*, *27*(5), 918–930, doi:10.2112/jcoastres-d-10-00088.1.
Mattias, A., C. E. Blenkinsopp, and G. Masselink (2014), Detailed investigation of overwash on a gravel barrier, *Mar. Geol.*, *350*, 27–38, doi:10.1016/j.margeo.2014.01.009.
McCallum, B. E., Wicklein, S. M., Reiser, R. G., Busciolano, R., Morrison, J., Verdi, R. J., Painter, J. A., Frantz, E. R., and Gotvald, A. J. (2013). Monitoring storm tide and flooding from Hurricane Sandy along the Atlantic Coast of the United States, October 2012 (No. 2013–1043, pp. 1–42), U.S. Geol. Surv.
McNamara, D. E., and A. Keeler (2013), A coupled physical and economic model of the response of coastal real estate to climate risk, *Nat. Clim. Change*, *3*(6), 559–562, doi:10.1038/NCLIMATE1826.
McNamara, D. E., and B. T. Werner (2008a), Coupled barrier island–resort model: 1. Emergent instabilities induced by strong human-landscape interactions, *J. Geophys. Res.*, *113*, F01016, doi:10.1029/2007JF000840.
McNamara, D. E., and B. T. Werner (2008b), Coupled barrier island–resort model: 2. Tests and predictions along Ocean City and Assateague Island National Seashore, Maryland, *J. Geophys. Res.*, *113*, F01017, doi:10.1029/2007JF000841.
Miselis, J., Andrews, B., Ganju, N., Navoy, A., Nicholson, R., and Defne, Z. (2013), Mapping, measuring, and modeling to understand water-quality dynamics in Barnegat Bay-Little Egg Harbor Estuary, New Jersey, *Sound Waves*. [Available at http://soundwaves.usgs.gov/2013/02/.]
Morton, R. A., and A. H. Sallenger Jr. (2003), Morphological impacts of extreme storms on sandy beaches and barriers, *J. Coastal Res.*, *19*, 560–573.
National Oceanic and Atmospheric Administration (2013a), NOAA tides and currents: Datums for 8534720, Atlantic City, N. J. [Available at http://tidesandcurrents.noaa.gov/datums.html?units=1&epoch=0&id=8534720&name=Atlantic+City&state=NJ.]
National Oceanic and Atmospheric Administration (2013b), NOAA water level and meteorological data report: Hurricane Sandy. [Available at www.tidesandcurrents.noaa.gov/publications/Hurricane_Sandy_2012_Water_Level_and_Meteorological_Data_Report.pdf.]
National Oceanic and Atmospheric Administration (2015), NOAA tides and currents. [Available at http://tidesandcurrents.noaa.gov/sltrends/sltrends.html/.]
Nordstrom, K. F. (1994), Beaches and dunes of human-altered coasts, *Prog. Phys. Geogr.*, *18*(4), 497–516, doi:10.1177/030913339401800402.
Overbeck, J. R., J. W. Long, H. F. Stockdon, and J. J. Birchler (2015), Enhancing evaluation of post-storm morphologic response using aerial orthoimagery from Hurricane Sandy, in *Coastal Sediments 2015*, edited by P. Wang and J. D. Rosati, World Scientific, Miami, Fla., doi:10.1142/9789814689977_0250.
Palmsten, M. L., and R. A. Holman (2012), Laboratory investigation of dune erosion using stereo video, *Coastal Eng.*, *60*, 123–135, doi:10.1016/j.coastaleng.2011.09.003.
Plant, N. G., and H. F. Stockdon (2012), Probabilistic prediction of barrier-island response to hurricanes, *J. Geophys. Res.*, *117*, F03015, doi:10.1029/2011JF002326.
Psuty, N. P. (2002), *Coastal Hazard Management: Lessons and Future Directions From New Jersey*, Rutgers Univ. Press, New Brunswick, N. J.
Redfield, A. C., and A. R. Miller (1955), *Water Levels Accompanying Atlantic Coast Hurricanes (No. R55 28)*, Woods Hole Oceanographic Institution, Mass.
Roelvink, D., A. Reniers, A. P. van Dongeren, J. V. T. de Vries, R. McCall, and J. Lescinski (2009), Modelling storm impacts on beaches, dunes and barrier islands, *Coastal Eng.*, *56*(11), 1133–1152, doi:10.1016/j.coastaleng.2009.08.006.
Sallenger, A. H., Jr. (2000), Storm impact scale for barrier islands, *J. Coastal Res.*, *16*(3), 890–895.
Sallenger, A. H., Jr., et al. (2003), Evaluation of airborne topographic lidar for quantifying beach changes, *J. Coastal Res.*, *19*, 125–133.
Sallenger, A. H., Jr., K. S. Doran, and P. A. Howd (2012), Hotspot of accelerated sea-level rise on the Atlantic Coast of North America, *Nat. Clim. Change*, *2*(12), 884–888, doi:10.1038/NCLIMATE1597.
Sallenger, A., W. Krabill, R. Swift, and J. Brock (2001), Quantifying hurricane-induced coastal changes using topographic lidar, in *Proceedings Coastal Dynamics 2001*, pp. 1007–1016, ASCE, Sweden.
Schoennagel, T., T. T. Veblen, and W. H. Romme (2004), The interaction of fire, fuels, and climate across Rocky Mountain forests, *BioScience*, *54*(7), 661–676, doi:10.1641/0006-3568(2004)054[0661:TIOFFA]2.0.CO;2.
Shaw, J., Y. You, D. Mohrig, and G. Kocurek (2015), Tracking hurricane-generated storm surge with washover fan stratigraphy, *Geology*, *43*(2), 127–130, doi:10.1130/G36460.1.
Sherwood, C. R., J. W. Long, P. J. Dickhudt, P. S. Dalyander, D. M. Thompson, and N. G. Plant (2014), Inundation of a barrier island (Chandeleur Islands, Louisiana, USA) during a hurricane: Observed water-level gradients and modeled seaward sand transport, *J. Geophys. Res. Earth Surf.*, *119*, 1498–1515, doi:10.1002/2013JF003069.
Stockdon, H. F., A. H. Sallenger Jr., J. H. List, and R. A. Holman (2002), Estimation of shoreline position and change using airborne topographic lidar data, *J. Coastal Res.*, *18*(3), 502–513.

Stockdon, H. F., K. S. Doran, and A. H. Sallenger Jr. (2009), Extraction of lidar-based dune-crest elevations for use in examining the vulnerability of beaches to inundation during hurricanes, *J. Coastal Res.*, 59–65, doi:10.2112/SI53-007.1.

Stocker, T. F., D. Qin, G. K. Plattner, M. Tignor, S. K. Allen, J. Boschung, A. Nauels, Y. Xia, V. Bex, and B. M. Midgley (2013), *IPCC, 2013: Climate Change 2013: The Physical Science Basis. Contribution of Working Group I to the Fifth Assessment Report of the Intergovernmental Panel on Climate Change*, Cambridge Univ. Press, Cambridge, U. K., and New York.

Thieler, E., E. A. Himmelstoss, J. L. Zichichi, and A. Ergul (2009). The Digital Shoreline Analysis System(DSAS) version 4.0—An ArcGIS extension for calculating shoreline change, U.S. Geol. Surv.

Titus, J. G., R. A. Park, S. P. Leatherman, J. R. Weggel, M. S. Greene, P. W. Mausel, S. Brown, C. Gaunt, M. Trehan, and G. Yohe (1991), Greenhouse effect and sea level rise: The cost of holding back the sea, *Coastal Manage.*, *19*(2), 171–204, doi:10.1080/08920759109362138.

Urquhart, E. A., M. J. Hoffman, R. R. Murphy, and B. F. Zaitchik (2013), Geospatial interpolation of MODIS-derived salinity and temperature in the Chesapeake Bay, *Remote Sens. Environ.*, *135*, 167–177.

Walters, D., L. J. Moore, O. Duran Vinent, S. Fagherazzi, and G. Mariotti (2014), Interactions between barrier islands and backbarrier marshes affect island system response to sea level rise: Insights from a coupled model, *J. Geophys. Res. Earth Surf.*, *119*, 2013–2031, doi:10.1002/2014JF003091.

Werner, B. T., and D. E. McNamara (2007), Dynamics of coupled human-landscape systems, *Geomorphology*, *91*(3), 393–407, doi:10.1016/j.geomorph.2007.04.020.

White, S. A., and Y. Wang (2003), Utilizing DEMs derived from lidar data to analyze morphologic change in the North Carolina coastline, *Remote Sens. Environ.*, *85*(1), 39–47, doi:10.1016/S0034-4257(02)00185-2.

Williams, H. F. L. (2015), Contrasting styles of Hurricane Irene washover sedimentation on three east coast barrier islands: Cape Lookout, North Carolina; Assateague Island, Virginia; and Fire Island, New York, *Geomorphology*, *231*, 182–192, doi:10.1016/j.geomorph.2014.11.027.

Wolinsky, M. A., and A. B. Murray (2009), A unifying framework for shoreline migration: 2. Application to wave-dominated coasts, *J. Geophys. Res.*, *114*, F01009, doi:10.1029/2007JF000856.

Wright, C. W., X. Fredericks, R. J. Troche, E. S. Klipp, C. J. Kranenburg, and D. B. Nagle (2014), *EAARL-B coastal topography*: *Eastern New Jersey*, *Hurricane Sandy*, *2012*: *First surface* (No. 767), U.S. Geol. Surv.

Zhang, K., and Z. Cui (2007), *Airborne Lidar Data Processing and Analysis Tools*, National Center for Airborne Laser Mapping, International Hurricane Research Center, Miami, Fla.

Zhang, K., and S. Leatherman (2011), Barrier island population along the U.S. Atlantic and Gulf Coasts, *J. Coastal Res.*, *27*(2), 356–363, doi:10.2112/JCOASTRES-D-10-00126.1.

Zhang, K., D. Whitman, S. Leatherman, and W. Robertson (2005), Quantification of beach changes caused by Hurricane Floyd along Florida's Atlantic Coast using airborne laser surveys, *J. Coastal Res.*, *21*, 123–134, doi:10.2112/02057.1.